4

Fully Coupled Surface–Subsurface Hydrological Modeling to Optimize Ancient Water Harvesting Techniques

Wim M. Cornelis[1], Koen Verbist[1,2], Tesfay Araya[3], Emmanuel Opolot[4], Jasmien C.J. Wildemeersch[1], and Bashar Al-Barri[1]

[1] *Department of Environment – UNESCO Chair for Eremology, Ghent University, Ghent, Belgium*
[2] *UNESCO, Enrique del Piano 2058, Santiago, Providenica, Chile*
[3] *Department of Agronomy, University of Fort Hare, Alice, South Africa*
[4] *Department of Agricultural Production, Makerere University, Kampala, Uganda*

4.1 Introduction

Worldwide, but particularly in drylands, water scarcity has become a major limitation to crop production and to delivering ecosystem services in general. Likewise, in many regions rainfall is becoming more erratic, with later and shorter rainy seasons, more and longer dry spells, and fewer rainy days (Sillmann et al. 2013), even in cases when total rainfall is increasing (Wu et al. 2013; Greve et al. 2014). This might be linked to anthropogenic climate change (Rockström and Falkenmark 2015). It results in a higher frequency of particularly agricultural droughts – shortage of available water for plant growth – which generally occur more often than meteorological droughts, i.e. shortage of precipitation (Wani et al. 2009).

In order to improve food and water security, water harvesting in its broadest sense should be an entry-point activity to enhance crop production through sustainable/ecological intensification. On a larger scale it contributes to regreening of the landscape, through crops, grasses, shrubs, or trees, hence rendering ecosystem services for society (Stroosnijder 2009). In a broad sense, water harvesting refers to retaining rainwater by in situ and ex situ practices (Dile et al. 2013; Cornelis 2014). In situ practices capture and store water where it falls, whereas ex situ practices collect water from a larger area and convey it to fields for immediate use or to storage systems for later use. Various examples are given elsewhere within this book.

Though such practices are often not new, dating back centuries or even millennia, and thus are based on grass-rooted knowledge, they are seeing a revival worldwide (Okhravi et al. 2019; Eslamian et al. 2017). Pandey et al. (2003) reported that throughout past civilizations, climate changes resulting in droughts were often followed by an increase in the use of water harvesting techniques, indicating that they can partly alleviate negative climatic conditions. They also stated that traditional systems would become more efficient if scientific attempts would be combined.

Recent developments in soil hydrology allow the use of complex distributed mechanistic models to describe hydrological processes at the field and catchment scale. These advances make it now feasible to use complex models to evaluate and improve ancient and present-day techniques. They assist in interpreting experimental results and operate as research tools for knowledge synthesis, in sharpening and cost reduction of lengthy and expensive field experiments, and in developing optimum strategic and tactic management practices (Steduto et al. 2009). Models are particularly helpful in evaluating potential management practices (*in casu* water harvesting techniques) and their design, and likely water balance and yield responses at specific sites before they are implemented (Cresswell et al. 2002). Through scenario analysis, they allow us to explore interactions between large numbers of management combinations, soils, and crops not only under historical weather conditions, including wet, normal, and dry years, but under future climates as well. This is not possible with traditional field experiments. Models are further very appropriate to evaluate the upstream and downstream hydrological impact of water harvesting techniques at the watershed scale. Harvesting water upstream can deprive downstream water users; vice versa, it can reduce flood risk (e.g. flash floods) or promote groundwater recharge and baseflow. Analyzing the potential and the implications of upscaling water harvesting on a watershed and/or

Handbook of Water Harvesting and Conservation: Case Studies and Application Examples, First Edition.
Edited by Saeid Eslamian and Faezeh Eslamian.

community scale is thus of primary importance. Outcomes of complex, distributed, mechanistic models, in replacement of tedious field experiments, can finally be useful in developing equations and determining parameter values for conceptual or engineering models.

This chapter describes a method to evaluate rainwater partitioning and compute water balance components as affected by water harvesting techniques, using a fully coupled surface–subsurface process-based hydrological model. The methodology will be illustrated with cases from Latin America (Chile) and sub-Saharan Africa (Ethiopia and Niger).

The Chilean case demonstrates how the model was used to simulate runoff and soil–water content near and below infiltration trenches (locally called *zanjas*) and how it was used to evaluate such existing practices at field scale (Verbist et al. 2012). It also illustrates that the model shows good performance when applied on the much larger scale of ~3 ha watersheds.

In Ethiopia, the model was used to evaluate and optimize conservation practices with broad and narrow permanent beds, which are modified versions of locally called *terwah* and *derdero* systems. This was done at a field scale by simulating soil moisture, runoff, and other water balance components, and relative yield (Opolot et al. 2016).

In a study in Niger, various water harvesting techniques were compared in terms of soil moisture redistribution, overland flow, and water balance components. Techniques included scarification, *zaï* pits, and microcatchments like semi-circular or half-moon bunds (*demi lunes*) (Wildemeersch et al. 2015b). Here we show an example of how overland flow, and infiltration and redistribution of water in the subsurface, can be simulated near a set of microcatchments.

The cases were selected as they cover different water harvesting techniques applied at different scales and agro-ecological zones, and were based on a variable degree of detail of model input parameters.

4.2 Fully Coupled Surface–Subsurface Modeling

There are several modeling approaches to evaluate hydrological impacts of water harvesting techniques. Some authors have used a conceptual approach with models such as SWAT (soil and water assessment tool) (Ouessar et al. 2009; Dile et al. 2013). Such models are, however, not much suitable for optimizing the design of water harvesting techniques. Others used a physical approach based on Richards' equation with, e.g. the Hydrus-2D code (Verbist et al. 2009), but such an approach does not enable us to simulate overland flow directly. Boers et al. (1986) combined the kinematic wave approximation for overland flow with the Richards equation (SWATRE code) for subsurface flow, but both processes were not fully coupled. Recently, Wesseling et al. (Ammar 2017) used a simple water balance-based rainwater harvesting model in MS Excel.

In this chapter, we demonstrate how the HydroGeoSPhere (HGS) code can be applied in a water harvesting context. HGS is capable of simulating surface–subsurface water flow in a three-dimensional framework using a fully integrated process-based finite-elements numerical approach (Sudicky et al. 2008; Therrien et al. 2010). It was originally developed to simulate surface–subsurface water flow and solute transport at a larger watershed scale. The model is based on a "blueprint for a physically based digitally simulated, hydrological response model" by R.A. Freeze and R.L. Harlan, which was developed in 1969 (Freeze and Harlan 1969).

As summarized in Opolot et al. (2016), the model uses a modified form of Richards' equation to describe 3D flow processes in the variably saturated subsurface:

$$-\nabla.(\omega_m q) + \sum \Gamma_{ex} \pm Q = \omega_m \frac{\partial}{\partial t}(\theta_s S_w) \tag{4.1}$$

where ω_m is the fraction of the total porosity occupied by the porous medium (dimensionless); this term is equal to 1 as long as only one porous continuum is considered for a simulation. The Darcian flux q ($L\,T^{-1}$) is given by:

$$q = -K_{sat}\, k_r(\psi)\nabla(\psi + Z) \tag{4.2}$$

where K_{sat} is the saturated hydraulic conductivity tensor ($L\,T^{-1}$), k_r represents the relative permeability of the medium in function of pressure head ψ (L) described by the Mualem-Van Genuchten function (Mualem 1976; Van Genuchten 1980), S_r is the degree of water saturation, and Z is the elevation or gravitational head (L). In Eq. (4.1), θ_s is the saturated soil–water content (dimensionless), and usually assumed to be equal to the porosity. Γ_{ex} ($L^3\,L^{-3}\,T^{-1}$) is the volumetric fluid exchange rate between the subsurface domain and all other types of domains supported by the model, Q ($L^3\,L^{-3}\,T^{-1}$) represents the fluid exchange with the outside of the simulation domain, specified by boundary conditions, and it is a volumetric fluid flux per unit volume representing a source or a sink to the porous medium system (Therrien et al. 2010).

Transient overland flow is described in 2D by the diffusion wave approximation of the Saint-Venant equation:

$$\frac{\partial \varphi_o \mathrm{h}_o}{\partial t} - \frac{\partial}{\partial x}\left(d_o K_{ox}\frac{\partial h_o}{\partial x}\right) - \frac{\partial}{\partial y}\left(d_o K_{oy}\frac{\partial h_o}{\partial y}\right) + d_o \Gamma_o \pm Q_o = 0 \tag{4.3}$$

where d_o is the depth of flow (L), h_o represents the water surface elevation (L), Γ_o is the volumetric exchange rate ($L^3L^{-3}T^{-1}$) between the surface flow and the subsurface flow, Q_o is a volumetric flow rate per unit area representing external sinks and sources (LT^{-1}), and φ_o is a surface flow domain porosity that, for flow over an uneven surface, varies between zero at the land surface and unity at the top of all rills and obstructions. This term is unity for flow over a flat plane. K_{ox} and K_{oy} are surface conductance (LT^{-1}) in x and y directions, respectively. These variables depend on the equation used to approximate the friction slopes (Therrien et al. 2010). For the cases demonstrated in this chapter, the Manning equation was used.

Surface and subsurface are coupled by means of the Darcy flux relation to transfer water from one layer to another. This is a general approach in which the Darcy flux is computed from the hydraulic head difference between surface and subsurface layers. It assumes that these two layers are separated by probably a thin layer of porous material through which water exchange occurs (Therrien et al. 2010). The exchange flux between the surface and subsurface layers is given by:

$$d_o\Gamma_o = \frac{k_r K_{zz}}{l_{exch}}(h - h_o) \tag{4.4}$$

where h_o and h represent the surface and subsurface water heads, respectively, k_r is the relative permeability for the exchange flux, K_{zz} is the vertical saturated hydraulic conductivity of the underlying layer, and l_{exch} is the coupling length which relates to the thickness of the assumed interface layer. A positive Γ_o represents an upward flow to the surface and a negative Γ_o implies otherwise (Therrien et al. 2010).

Interception and evapotranspiration processes are simulated based on equations developed by Kristensen and Jensen (1975) and Wigmosta et al. (1994). A full description of these equations and the HGS model in general can be found in Therrien et al. (2010). A bucket type model is used to simulate the interception process whereby only precipitation in excess of interception storage (L) and evaporation reaches the soil surface. The amount of water stored by the interception process varies between zero and a maximum (S_{int}^{Max}). According to Kristensen and Jensen (1975), this factor depends on vegetation type and stage of development and is calculated as:

$$S_{int}^{Max} = C_{int}LAI \tag{4.5}$$

where C_{int} is the empirical canopy storage parameter (L) and LAI is the dimensionless leaf area index. Rainfall and evaporation are the processes that, respectively, fill and deplete the interception storage.

Evapotranspiration is simulated as a combination of plant transpiration and evaporation processes that affect both surface and subsurface flow domains. Transpiration T_p is influenced by vegetation, soil-water content and the root distribution function. It occurs within the root zone of the subsurface and is calculated as (Kristensen and Jensen 1975):

$$T_p = f_1(LAI)\, f_2(\theta) RDF(E_p - E_{CAN}) \tag{4.6}$$

where f_1(LAI) is a function of LAI (−), $f_2(\theta)$ is a function of nodal water content (−), RDF is the time-varying root density function (−), E_p is the potential evapotranspiration (LT^{-1}) and E_{CAN} is the evaporation of the intercepted water by the canopy (LT^{-1}). The vegetation parameter, f_1(LAI), is given as:

$$f_1(LAI) = \max\{0, min[1, (C_2 + C_1 LAI)]\} \tag{4.7}$$

where C_1 and C_2 are empirical constants, with respective standard values of 0.5 and 0.

The root density function, RDF, is defined as:

$$RDF = \frac{\int_{z_1'}^{z_2} r_{F(Z')\mathrm{d}z'}}{\int_0^{L_r} r_{F(Z')\mathrm{d}z'}} \tag{4.8}$$

where L_r is the effective root length (L), z' is the depth from the soil surface (L), and $r_F(z')$ is the logarithmic root extraction function. The RDF can be linear, quadratic, or cubic function or a constant value can be taken (Therrien et al. 2010). In this chapter a constant value of 1 recommended for shallow depth crops (Feddes and Raats 2004) was used.

The soil–water content dependence term $f_2(\theta)$ relates the transpiration to different saturation degrees, with the maximum value between the soil–water content at field capacity θ_{fc} and the oxic limit θ_{ox}, while decreasing to zero at the wilting point soil–water content θ_{wp} and the anoxic limit θ_{an}:

$$f_2(\theta) = \begin{cases} 0 \;\; for \;\; 0 \le \theta \le \theta_{wp} \\ f_3 \, for \, \theta_{wp} \le \theta \le \theta_{fc} \\ 1 \;\; for \;\; \theta_{fc} \le \theta \le \theta_{ox} \\ f_4 \;\; for \;\; \theta_{ox} \le \theta \le \theta_{an} \\ 0 \;\; for \;\; \theta_{an} \le \theta \end{cases} \tag{4.9}$$

where

$$f_3 = 1 - \left[\frac{\theta_{fc} - \theta}{\theta_{fc} - \theta_{wp}}\right]^{C_3} \tag{4.10}$$

and

$$f_4 = 1 - \left[\frac{\theta_{an} - \theta}{\theta_{an} - \theta_o}\right]^{C_3} \tag{4.11}$$

The dimensionless fitting parameter C_3 determines the rate of $f_2(\theta)$ change with θ, and becomes linear for C_3 equal to 1, as is commonly assumed.

Table 4.1 Model parameters needed in HGS.

Process	Parameter	Source
Surface-subsurface flow	Field saturated hydraulic conductivity K_{sat}	Field measured, calibrated
	Van Genuchten water retention curve parameters (θ_s, θ_r, α, n)	Lab measured, calibrated
	Mualem's shape parameter l	Literature
	Coupling length l_{exch}	Calibrated
	x- and y-friction factor	Literature (Manning n tables)
Evapotranspiration	Transpiration fitting parameters (C1, C2, C3)	Literature
	Transpiration limiting saturations (θ_{fc}, θ_{wp}, θ_{ox}, θ_{an})	Literature
	Evaporation limiting saturations (minimum, maximum, LAI, root zone depth, evaporation depth, canopy storage parameter, initial interception storage)	Field measured, literature

The soil–water evaporation, E_s is calculated in the cases presented here by:

$$E_s = \alpha^*(E_p - E_{CAN})[1 - f_1(LAI)]EDF \tag{4.12}$$

where α^* is the wetness factor that is used to describe the moisture availability for the subsurface domain (Allen et al. 1998). *EDF* is the evaporation distribution function describing the reduction of the energy penetration with depth (Therrien et al. 2010).

Input parameter values to describe surface–subsurface flow were derived from field measurements (K_{sat}) and lab analysis on undisturbed soil cores (van Genuchten parameters of the water retention curve), optimized within the model calibration process as outlined in the next sections. The parameter values used for the simulation of evapotranspiration and interception were taken from literature, except for water content at field capacity and permanent wilting point, which were taken from the optimized water retention curves. Table 4.1 gives an overview of all parameters needed and how they were assessed.

4.3 Infiltration Trenches in Chile

Field experiments were performed in Chile at two locations. Location 1 was a sandy loam hillslope (Typic Thorriorthent, Soil Taxonomy) in the greater Elqui Valley, characterized by an arid Mediterranean climate (with 99 mm of annual precipitation and a reference evaporation of 1500 mm) where a governmental body had laid out infiltration trenches (*zanjas*) prior to our study to promote recovery of natural vegetation and reduce land degradation (Figure 4.1). Location 2 comprised two ~3 ha watersheds with loamy soil in the semi-arid Metropolitan Region (annual precipitation is 560 mm and reference evaporation 1220 mm). One watershed had been managed (with infiltration trenches) for the same reasons as in location 1 while the other was not managed (without trenches) (Figure 4.1). For details on how the model was parameterized, the reader is referred to Verbist et al. (2012).

At location 1, a field plot of 6×2 m was selected on hillslope with a 23% slope and consisted of an infiltration trench of $2 \times 0.4 \times 0.25$ m with its impluvium (9.2 m^2). Twenty-two 30 cm-long Time Domain Reflectometry (TDR) probes, connected to a Campbell Scientific TDR100 device and CR10X datalogger, were installed horizontally at 0.07, 0.15, 0.30, and 0.45 m below the soil surface. Only those probes that recorded changes in soil–water content were used for model calibration. Figure 4.2 shows the location of the final set of nine withdrawn probes. A rainfall event with an intensity of 120 mm h^{-1} was simulated for 20 minutes using a rainfall simulator similar to the one described by Verbist et al. (2003). During the simulated 20 minute-long rainfall event, the advance of the wetting front was monitored with the TDR probes and soil–water content was further monitored after the rainfall event until no significant changes were observed for a 24-hour period, which was four days from the start of the rainfall simulation. Runoff discharge exiting the parcel was guided by a funnel through a 1 m-long plastic tube and was measured at one-minute intervals using calibrated beakers of 700 cm^3.

Soil–water retention characteristic curves were determined on 25 undisturbed soil samples taken using standard sharpened steel 100 cm^3 Kopecky rings at various depths (0–5 cm, 15–20 cm, 25–30 cm, and 35–40 cm) at 1 m intervals along the slope. Constant-head infiltration measurements were performed at the selected field plot to quantify

Figure 4.1 Hillslope with impluvium, infiltration trench, and 10 m-long rainfall simulator in the Elqui Valley, Chile (left), and watersheds with (front) and without (back) infiltration trenches in the Metropolitan Region, Chile (right).

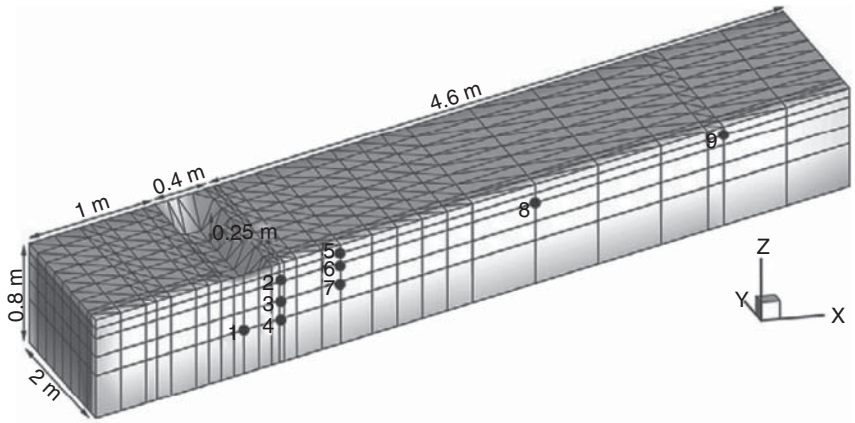

Figure 4.2 Location of trench and TDR probes, and 3D grid of the test area.

the field unsaturated and saturated hydraulic conductivity. More details are given in Verbist et al. (2009, 2010b).

A comparable procedure was followed at location 2, but with soil sampling and infiltration measurements taken at, respectively, five and two locations along three transects (Baetens et al. 2009). Additionally, runoff discharge of the complete watershed was recorded with a limnigraph with a V-shaped weir at the outlet of each watershed.

Based on detailed measurements of the geometry of the slope and trench, a 2D grid was generated using Grid Builder (McLaren 2007). In order to more accurately represent field conditions, a variable grid density was chosen with small grid elements forming the trench area and larger grid elements shaping the catchment area. The 3D grid was then generated by extending the 2D grid to greater depths. Figure 4.3 shows the 2D grid at the 3 ha watershed (location 2), with a refinement near the river and infiltration trenches, and a 3D visualization of the surface elevation (based on a DEM [digital elevation model] and kriging) in which the trenches are clearly detectable. Figure 4.2 shows the grid used for the study at location 1.

Because of the parameter interaction that typically occurs in a highly parameterized non-linear model such as the one used, a variance-based global sensitivity analysis (GSA) was applied on the arid hillslope (small catchment) dataset (rather than a local sensitivity analysis or one-at-a-time approach). GSA looks at both the first order sensitivities as well as the total order sensitivities starting from the model output variance (Verbist et al. 2012). Since prior studies on inverse modeling of unsaturated flow identified the need to supply at least two different data types to calibrate unsaturated flow models uniquely (e.g. Wöhling and Vrugt 2011), two different model outputs, i.e. runoff hydrographs and soil–water content time series, were used in the inversion process to parameterize HGS. As GSA showed that model output was most sensitive to K_{sat}, the van Genuchten parameters θ_s, α and n (describing the water retention curve), and the coupling length l_{exch} of the impluvium and the trench, these parameters were selected for optimization in calibrating HGS. This was done with the Parameter ESTimation software PEST (Doherty 2010). Details can be found in Verbist et al. (2012).

Figure 4.4 shows that at location 1 observed and simulated soil–water contents and runoff match very well. The simulated runoff downslope of the trench (after 14 minutes; dashed line) perfectly accorded with the observed overtopping. This is an important feature of the model, since it allows representing interaction of water harvesting techniques in complex design schemes. As such, a better

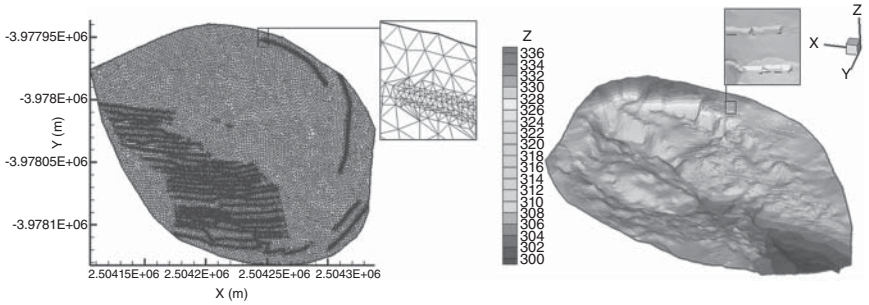

Figure 4.3 2D grid at the 3 ha watershed, with a refinement near the river and infiltration trenches (left) and 3D visualization of the surface elevation (in m) (right). Small windows illustrate the trenches.

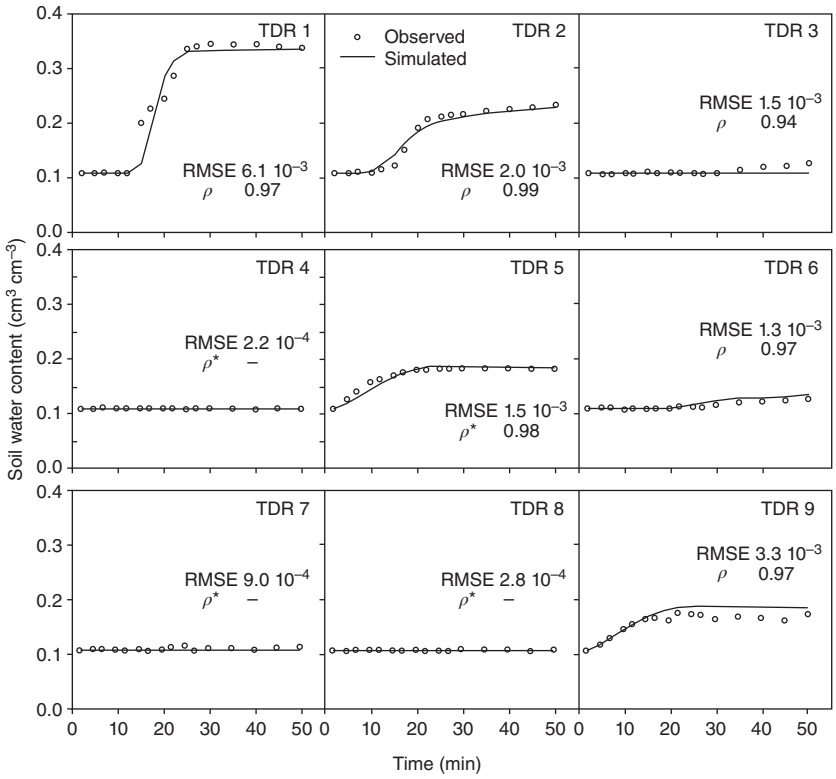

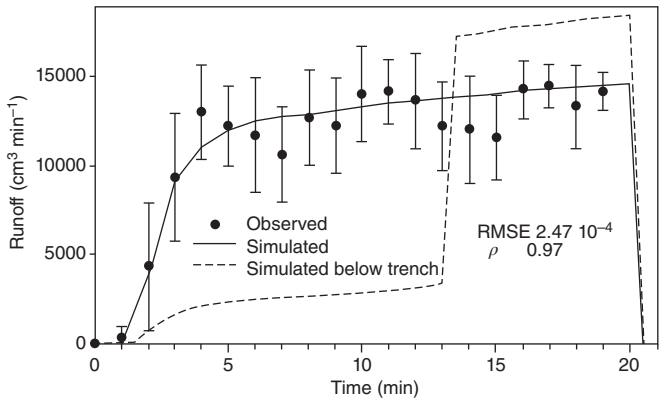

Figure 4.4 Observed (dots) and simulated (line), top panel, soil–water content for nine TDR probes inserted under the impluvium and trench, and, bottom panel, runoff influx into trench (continuous line) and runoff downhill of the trench (dashed line) with time at location 1. The hydrograph "below trench" clearly shows the overtopping of the trench 14 minutes after the start of the rainfall. RMSE is root mean square error and ρ is Pearson correlation coefficient. The whiskers indicate the standard deviation on the measured runoff values. The locations of each TDR probe are shown in Figure 4.2.

understanding of the behavior and effectiveness of these water harvesting techniques on irregular terrains becomes feasible (Verbist et al. 2012).

To evaluate rainwater harvesting efficiency, the calibrated model (Verbist et al. 2012) was used to simulate runoff and redistribution of soil water at location 1 for a slope with and without a trench under the same simulated rainfall conditions (Figure 4.5). Visually, large differences in water content (expressed as degree of saturation) are apparent between both cases. When looking at the cross-section

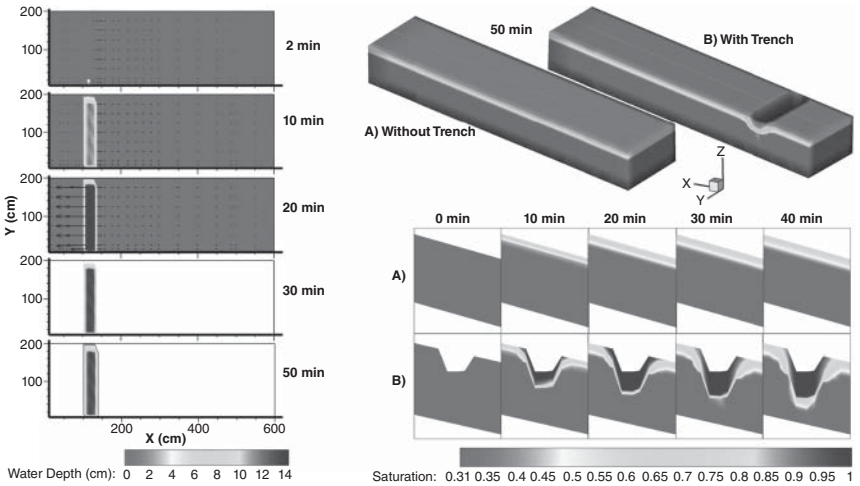

Figure 4.5 Left panel: 2D representation of the simulated water depth at the soil surface and in the trench at times 0–50 minutes. Vectors indicate the overland flow direction and velocity at the node level. Note that the color scale starts at a water depth of 1×10^{-5} cm. A white color thus means a zero water depth and no overland flow. Right panel: 3D representation of the simulated soil–water content expressed as saturation degree (a) without and (b) with water harvesting trench at time 50 minutes. The lower part shows a vertical 2D slice of the soil domain at y = 100 cm and at time 0–40 minutes.

along the slope at the middle position ($y = 1$ m), the water harvesting capacity of the trench becomes clear, with increased water storage in the soil domain surrounding the trench, when compared to the unaltered slope (Verbist et al. 2012). The very local effect of water storage in infiltration trenches was also observed by Makurira et al. (2007).

At location 1, for a total rainfall amount of 36.9 mm applied during the rainfall simulations, 63% was lost by runoff when no trench was present (23.2 mm), whereas only 12.5 mm of runoff was generated in the case with the trench. This decrease in runoff by 46% means that, for the simulated rainfall, 10.7 mm (29%) of additional runoff water infiltrated in the soil profile when a trench was present. However, when extending the evaluation of the infiltration trenches' efficiency to natural rainfall conditions occurring in the area of interest, the model demonstrated that for dry, normal, and wet years (22, 58, and 102 mm, resp.), the volumetric differences of the water balance components between both cases were very small (Verbist et al. 2012).

Actual transpiration and soil evaporation were clearly driven by precipitation constraints, increasing from dry to wet. The observed precipitation in those years was indeed below the minimum precipitation for optimal microcatchment runoff water harvesting, which has been estimated to lie between an annual precipitation amount of 100 mm (Boers and Benasher 1982) and 250 mm (Chritchley and Siegert 1991). Only under extremely wet conditions did differences in the water balance components become apparent. In the wettest year on record (1940–2008) with 407 mm annual rainfall (1987) due to a strong El Niño signal (Verbist et al. 2010a), the infiltration trenches resulted in a 65% reduction in runoff. However, with infiltration trenches soil–water content only increased by 9% in 1987, as a large part of the infiltrating water was lost to deep drainage (below 0.8 m) (+189%). This means that although infiltration trenches have a great potential to harvest water, they were not efficient in retaining water in the soil under the climatic and soil conditions prevailing in this arid study area (Verbist et al. 2012). Yet, as they potentially can greatly reduce runoff, they will contribute to reducing transport of sediment from the watershed, especially under high rainfall events.

At location 2, runs with the model calibrated for the semi-arid watersheds of interest were made for several years. Figure 4.6 shows a reasonable agreement between observed and simulated runoff at the watershed outlet (3 to 15 October 1997, with 1997 being a wet year). Although the watershed with infiltration trenches has an extremely complex microtopography because of the presence of hundreds of trenches, the general runoff pattern was well captured (Cornelis et al. 2012).

Simulations for dry, normal, and wet years (144, 438, and 893 mm, resp.) showed that the presence of the infiltration trenches in the watershed reduced runoff by 14–23% (Cornelis et al. 2012). To further improve their efficiency in reducing runoff and promoting rainwater infiltration, different design scenarios in terms of trench dimensions and distance between multiple trenches could be developed.

4.4 Broad and Narrow Beds in Ethiopia

Field experiments were conducted in Tigray, northern Ethiopia, on clayey Pelli Calcic Vertisols (WRB [World Reference Base]). The climate at the study site is cool tropical semi-arid with recurrent droughts (with mean annual rainfall of 512 mm and mean reference evapotranspiration of 1486 mm). More than 85% of rain falls during the cropping season from mid-June to mid-September (Araya et al. 2011). In this study, teff (*Eragrostis tef*) and wheat (*Triticum* spp.) were grown in cropping seasons of 2009

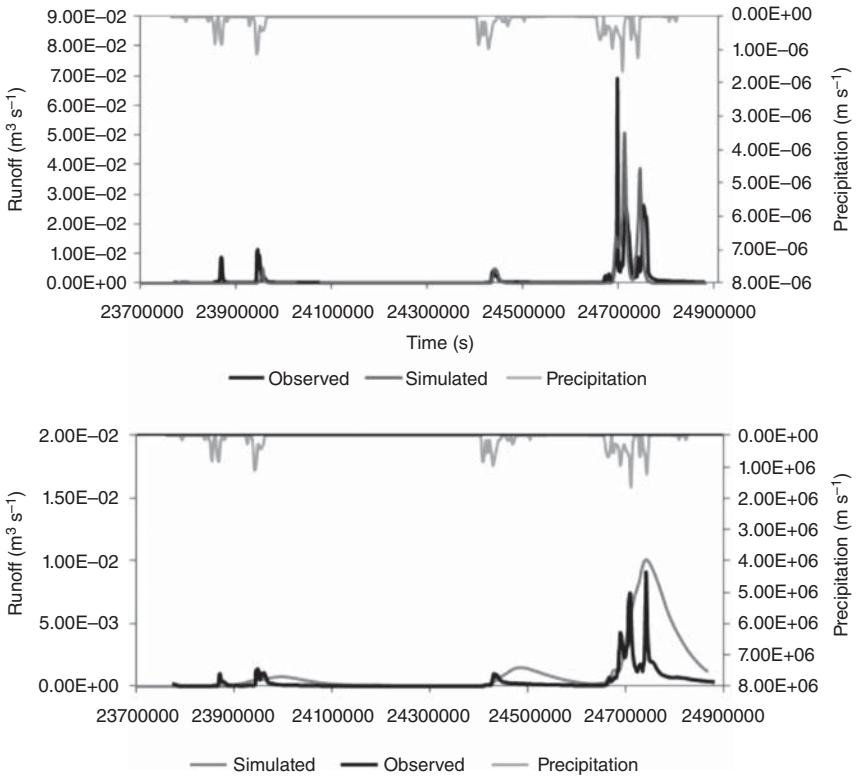

Figure 4.6 Observed and simulated runoff at the watershed outlet with (top) and without (bottom) infiltration trenches (3–15 October 1997).

and 2010 and were considered during model calibration and verification, respectively. Frequency analysis showed that 2009 was drier than normal, and 2010 wetter.

Two grass-rooted water harvesting practices, modified as described below, were tested in comparison with conventional farmers' practices on a farmer's field with a 3% slope. Plots of 19 × 5 m were laid out in three replicates. In the *terwah* + practice, 0.2 m wide and 0.1 m deep contour furrows were created at 1.5 m intervals between permanent broad beds to collect excess water. In *derdero*+, permanent raised beds of 0.6 m width with 0.2 m wide and 0.1 m deep furrows were created to prevent water logging and collect excess water that would otherwise runoff. The plus sign (+) in both practices represents retaining at least 30% of crop residue after a cropping season, minimum tillage of the beds and crop rotations to comply with the principles of conservation agriculture (Araya et al. 2011) (Figure 4.7). Detailed measurements of the geometry of the slope and the beds and furrows were used to generate a 3D grid using Grid Builder (McLaren 2007). Two layers (base and top) were first generated for each plot, with the top layer being further transformed to include furrows of 0.2 m wide and 0.1 m deep at regular intervals of 1.5 and 0.6 m for TER+ and DER+, respectively. Finer grids (0.05 × 0.05 m) were used at the furrows. The 2D grids were then extended to a depth of 1 m to generate the 3D grids (Figure 4.8).

Soil–water retention curves were established from three undisturbed soil samples taken from each plot using standard sharpened steel 100 cm^3 Kopecky rings at different depths of 0–10 cm, 10–20 cm, and 30–40 cm. Similar soil samples were also taken outside the experimental plots at depths of 50–60 cm, 70–80 cm, and 90–100 cm. Field saturated hydraulic conductivity was obtained from constant-head infiltration tests (Araya et al. 2016).

Runoff and soil moisture was measured under natural rainfall conditions. The major challenge faced during the calibration and validation of the model was lack of detailed measurements of rainfall intensity data for the complete period under study (Opolot et al. 2016). An assumed average rain intensity value based on measurements taken in the study area between 4 July and 21 August 2009 was used and incorporated into the measured daily rainfall (Opolot 2012). Runoff was determined from trenches of about 4.5 m long, 1.5 m wide, and 1 m deep dug at the lower end of each plot and lined with 0.5 mm thick plastic sheets for runoff and sediment collection. The average water height in each trench was taken every morning after the rainfall event that generated runoff.

The soil–water content was measured gravimetrically with five to seven day intervals on soil samples taken in three replicates for each treatment at 20 cm intervals up to a depth of 1 m using an auger (Araya et al. 2015). Fresh weights of these samples were taken in the field

Figure 4.7 Field trials in Tigray, Ethiopia, with *derdero+* in the forefront.

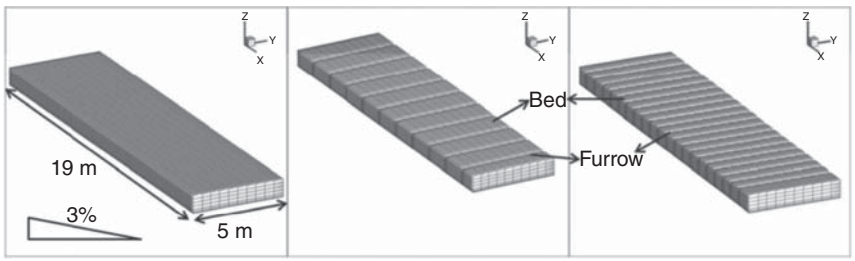

Figure 4.8 Model setup of conventional tillage (left), *terwah+* (middle), and *derdero+* (right) water harvesting practices. Source: Opolot et al. (2016).

before they were transported to the laboratory. Samples were oven-dried at 105 °C for 24 hours and their dry weights were measured. Volumetric soil–water content, θ was obtained from gravimetric soil–water content and bulk density using the soil shrinkage characteristic curve equation suggested by Cornelis et al. (2006). Volumetric soil–water content was concurrently recorded until 1 m depth using a Trime® water sensor (IMKO Micromodultechnik GmbH, Germany), which is a dielectric method. However, the data appeared to be unreliable in the swelling and shrinking clay soil under study (Araya et al. 2015) and were therefore not further used in this study.

PEST software (Doherty 2010) was used for automatic parameter optimization where for each model run, the measured values of 2009 were compared with the simulated values. A previous study by Verbist et al. (2012; Section 4.3) showed that both surface runoff and soil–water content simulation were most sensitive to coupling length l_{exch} and K_{sat}. These authors also showed that subsurface water redistribution was sensitive to Van Genuchten parameters α, n, and θ_s, but in this study, α and n were kept to their initial values and only l_{exch}, K_{sat}, and θ_s were optimized. This was done to avoid overparameterization of the model given the fewer observed data being available compared to the study of Verbist et al. (2012). Both runoff and soil–water contents were used in the optimization process and enabled an evaluation of the model capacity to optimize both surface and subsurface processes simultaneously using appropriate weighting (Opolot et al. 2016). For *derdero+* this resulted in simulated soil-water content as compared to observations in a RMSE (root mean square error) of 0.03 m^3 m^{-3}, a Pearson correlation coefficient of 0.84, and a Nash-Sutcliffe model efficiency coefficient E of 0.60. For runoff, the values were 0.95 mm, 0.88, and 0.58 (Opolot et al. 2016). These results are acceptable.

As a validation based on 2010 data, Figures 4.9 and 4.10 show good agreement between simulated (using the calibrated model) and observed runoff and soil–water content values, respectively, for *derdero+* tillage practices following rainfall events from 20 July until 2 September 2010. For soil–water content, RMSE was 0.03 m^3 m^{-3}, the Pearson correlation coefficient 0.93, and the Nash-Sutcliffe model efficiency coefficient E 0.83. For runoff, the values were 1.15 mm, 0.92 and 0.70. Similar results were obtained for the *terwah+* practices (Opolot et al. 2016).

Simulated water balance components for dry, normal, and wet years for each water harvesting practice under wheat are summarized in Table 4.2 (Opolot et al. 2016). These results indicate that the *derdero+* practice results in low runoff generation followed by *terwah+*, while conventional practices are associated with higher runoff generation across all the years. For example, about 8% of

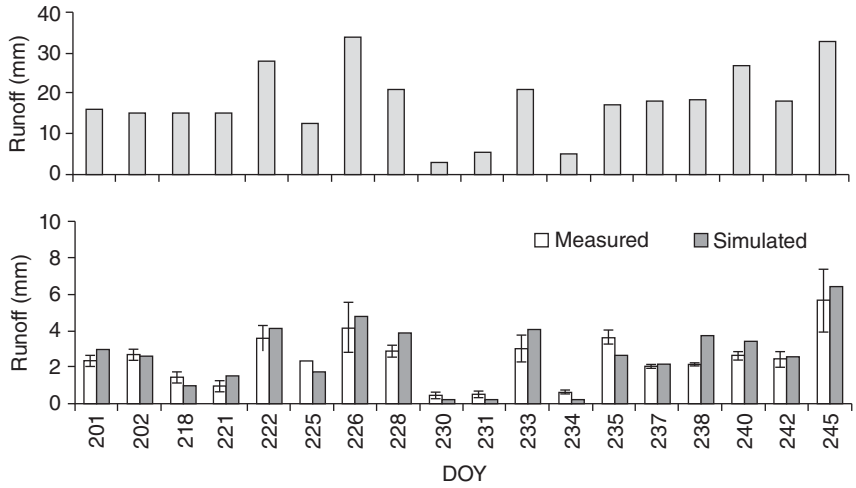

Figure 4.9 Precipitation and comparison between HGS simulated runoff and measured runoff for *derdero*+ using the 2010 validation dataset. The error bars show the standard error of the mean of measured values. DOY 201 and 245 correspond to 20 July 2010 and 2 September 2010, respectively. DOY is day of the year from the Julian calendar. Source: Opolot et al. (2016).

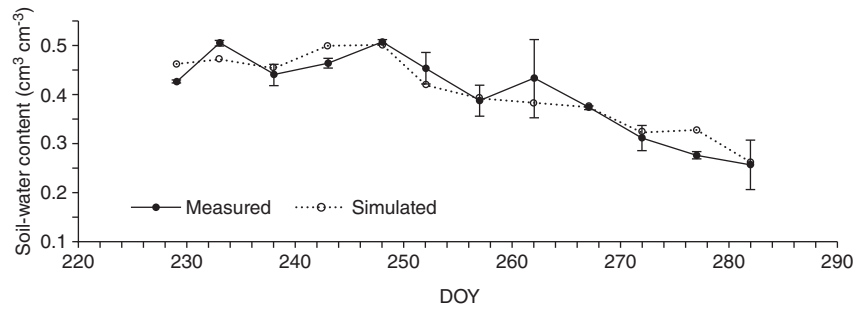

Figure 4.10 Comparison between HGS simulated and measured soil-water content at 0.15 m for *derdero*+ using the 2010 validation dataset. The error bars show the standard error of the mean of measured values. The period of simulation was between 17 August 2010 (DOY = 229) and 9 October 2010 (DOY = 282). DOY is day of the year from the Julian calendar.

Table 4.2 Soil water balance components for *derdero*+ DER+, *terwah*+ TER+, and conventional tillage (CT) practices calculated for dry and wet years in the Ethiopian highlands, Tigray, Ethiopia.

Year	Condition	Treatment	P	RO	T_p	E_s	E_p	D	ΔS
			mm						
2005	Dry	DER+	287	8	17	17	2	0	243
		TER+	287	8	38	25	0	0	217
		CT	287	36	8	12	0	0	230
2006	Wet	DER+	541	50	22	57	9	237	166
		TER+	541	67	20	44	3	184	223
		CT	541	160	10	38	0	0	333
2009	Dry	DER+	355	20	27	40	0	0	269
		TER+	355	46	50	23	0	0	237
		CT	355	95	12	18	0	0	230
2010	Wet	DER+	500	41	45	81	5	64	264
		TER+	500	38	37	70	1	131	223
		CT	500	155	12	34	0	1	298

Calculations are made for a four-month growing season, i.e. from June to September. All calculations were based on the four months (June to September) of the growing season. P is rainfall, RO is runoff, Tp is actual transpiration, Es is soil evaporation, Ep is surface evaporation, D is deep drainage, ΔS is change in water storage, DER+ is *derdero*+, TER+ is *terwah*+, CT is conventional tillage.
Source: Opolot et al. (2016).

the rainfall P was lost as runoff RO under *derdero*+ and *terwah*+ compared to 31% under conventional practice in the wet year of 2010. Simulated results indicate deep percolation D (below 1 m) as the main unproductive water loss only in wet years especially for *derdero*+ and *terwah*+. For example, it was highest under *terwah*+ (131 mm) followed by *derdero*+ (64 mm), whereas the lowest value (1 mm) was recorded under the conventional practice in

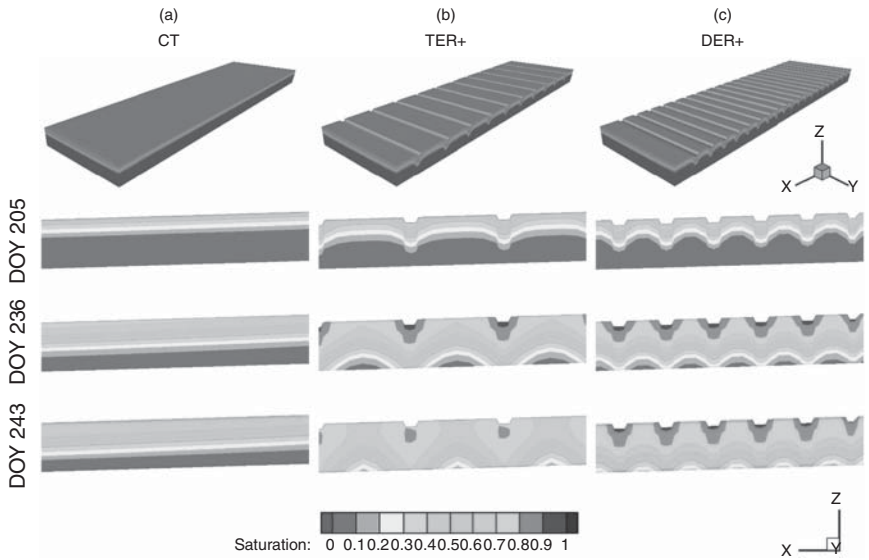

Figure 4.11 Upper panel: 3D representation of simulated soil–water content expressed as saturation degree as influenced by conventional tillage CT (a), *terwah*+ TER+ (b) and *derdero* + DER+ (c) on DOY 205 (2010) following a total rainfall of 15 mm. Lower panel: vertical 2D slice of the soil domain at a point, y = 2.5 m showing simulated water content expressed as saturation degree at three different dates in 2010. These three dates represent different rainfall events; after a rainfall event of 15 mm (DOY 205) and after a rainfall event of 21 mm (DOY 236). No rainfall event was recorded on DOY 243, but at total rainfall of 49 mm was received between DOY 237 and DOY 243. Notice higher water content indicated by the saturation degree (blue color) in DER+ closely followed by TER+. DOY is day of the year from the Julian calendar. Source: Opolot et al. (2016).

the growing season of 2010. More details about the other water balance components can be found in Opolot et al. (2016).

Redistribution of soil moisture under wheat as influenced by *derdero*+ and *terwah*+ tillage practices can be clearly visualized in Figure 4.11 for the year 2010 (Opolot et al. 2016). From the 3D representation it can be seen that *derdero*+ has more soil moisture distributed throughout the root zone due its closely spaced furrows. *Terwah*+ is as well more effective than conventional tillage as the furrows collect water and slowly distribute it into the lower soil depth (DOY [day of year] 205 and DOY 236).

The model could be further used to compute relative yields, i.e. actual yield Y_a over potential/maximum yield Y_m (Y_a/Y_m), of crops as influenced by the water harvesting techniques (results not shown; see Opolot et al. 2016). As expected, simulated Y_a/Y_m values were higher in wet and normal years compared to those of a dry year. Relative differences between the techniques were highest in dry years; however, in wet years the water harvesting techniques also sometimes resulted in higher relative yields as they improve drainage and thus minimize waterlogging. In general, relative yields were highest under *derdero*+, followed by *terwah*+ and least under conventional tillage.

The model was also used to test water harvesting design optimization. The idea was that deeper furrows would increase the ponding time and consequently reduce runoff and increase water infiltration into the soil. The technique that takes this new modification into account has been renamed as *seleste derdar* (Lanckriet et al. 2014). This study thus tested the effect of increasing furrow depth from the 0.10 m currently used to about 0.15 m (i.e. shift from *derdero*+ to *seleste derdar*). Simulation results for the wet year 2010 indicate that only 3% of the rainfall was lost as runoff under *seleste derdar*. Other modifications to the water harvesting techniques were tested as well, but are not shown here (see Opolot 2012). These findings demonstrate an even greater potential of the water harvesting practices to reduce surface runoff and thus enhance the availability of water to plants if farmers are able to reshape their furrows to an appropriate depth. They also show the great potential of such a modeling approach (in which a mechanistic model was calibrated and validated based on data collected from a limited number of field experiments) to test various designs by performing synthetic experiments, rather than testing them in (a limited number of) field experiments under a small range of weather and environmental conditions.

4.5 Microcatchments in Niger

In Niger, a field experiment was set up on a Plinthosol (WRB) in the Tillaberí region with shallow (30 cm) sandy topsoil. The field site forms part of a typical toposequence

of the Sahelian "inverted" landscape and belongs to "marginal lands." The region is located in the southern, wettest part of the country where most agricultural activity takes place (below the 400 mm isohyet). The climate is Sudano-Sahelian with a long, hot and dry season (November–May), and a short cropping season (June–October). Rainfall has an annual average of 550 mm and is highly variable in space and time. Reference evapotranspiration varies between 2000 and 2500 mm (Sivakumar 1989).

Three water harvesting techniques were tested and compared with a control on a field with 1% slope. Scarification practice was based on farmers' suggestions and instructions of key informants specializing in local soil and water conservation techniques. Half-moon (*demi lunes*) microcatchments and *zaï* pits have been extensively described in scientific literature, and were therefore tested as well. More details can be found in Wildemeersch et al. (2015b). Figure 4.12 illustrates the three water harvesting techniques tested.

Soil–water retention curves were established using 45 undisturbed soil samples taken from each plot with standard sharpened steel 100 cm^3 Kopecky rings at depths of 0–5 cm and 5–10 cm. Field saturated hydraulic conductivity was obtained from constant-head infiltration tests (Wildemeersch et al. 2015b).

Runoff and soil moisture was measured under natural rainfall conditions. Soil–water content was monitored from 2011 to 2012 using a neutron probe (CPN-503DR hydroprobe) with two aluminum access tubes installed per plot. One was positioned near the crop (pearl millet, *Pennisetum glaucum*), which, in the case of the *zaï*, microcatchment and scarification treatments entails the pit, half-moon, and trench, respectively, and one was placed in between plants or catchments (Wildemeersch et al. 2015a). In 2013, each plot was equipped with a runoff collecting system at its downslope end (Wildemeersch 2014). Due to political instability in the region in 2013, data from that year could not be properly collected and 2013 was further omitted in this study. Unlike the studies described in Sections 4.3 and 4.4, the model was therefore calibrated and validated with soil–water content data only, collected in 2011 and 2012. Model calibration was performed with PEST software (Doherty 2010). A moderate to good agreement between simulated and observed soil-water content values in and outside the pit, half-moon, or trench was observed with RMSE varying between 0.02 for the control and 0.1 $m^3\ m^{-3}$ for the half-moon microcatchments (Wildemeersch 2014). Model performance could have been improved when runoff data would have been used in addition to the soil–water content data.

Figure 4.13 shows simulated (a, left panel) water depth (overland flow) and (b, right panel) degree of saturation (subsurface flow) at different time steps following a rainfall event initiated at 07h on DOY 220 (40 mm) in 2011, for the

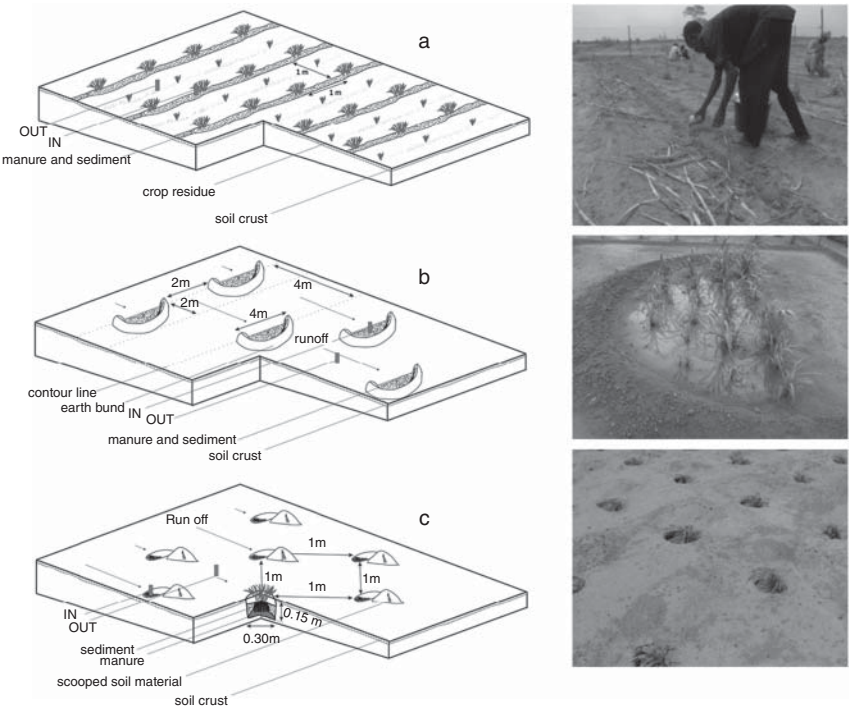

Figure 4.12 Water harvesting techniques evaluated on the experimental field, with (a, upper panel) scarification, (b, middle panel) half-moon microcatchments, and (c, lower panel) *zaï* pits. IN and OUT refer to access tubes for measuring soil–water content with a neutron probe in and out of the half-moon microcatchment or *zaï* pit.

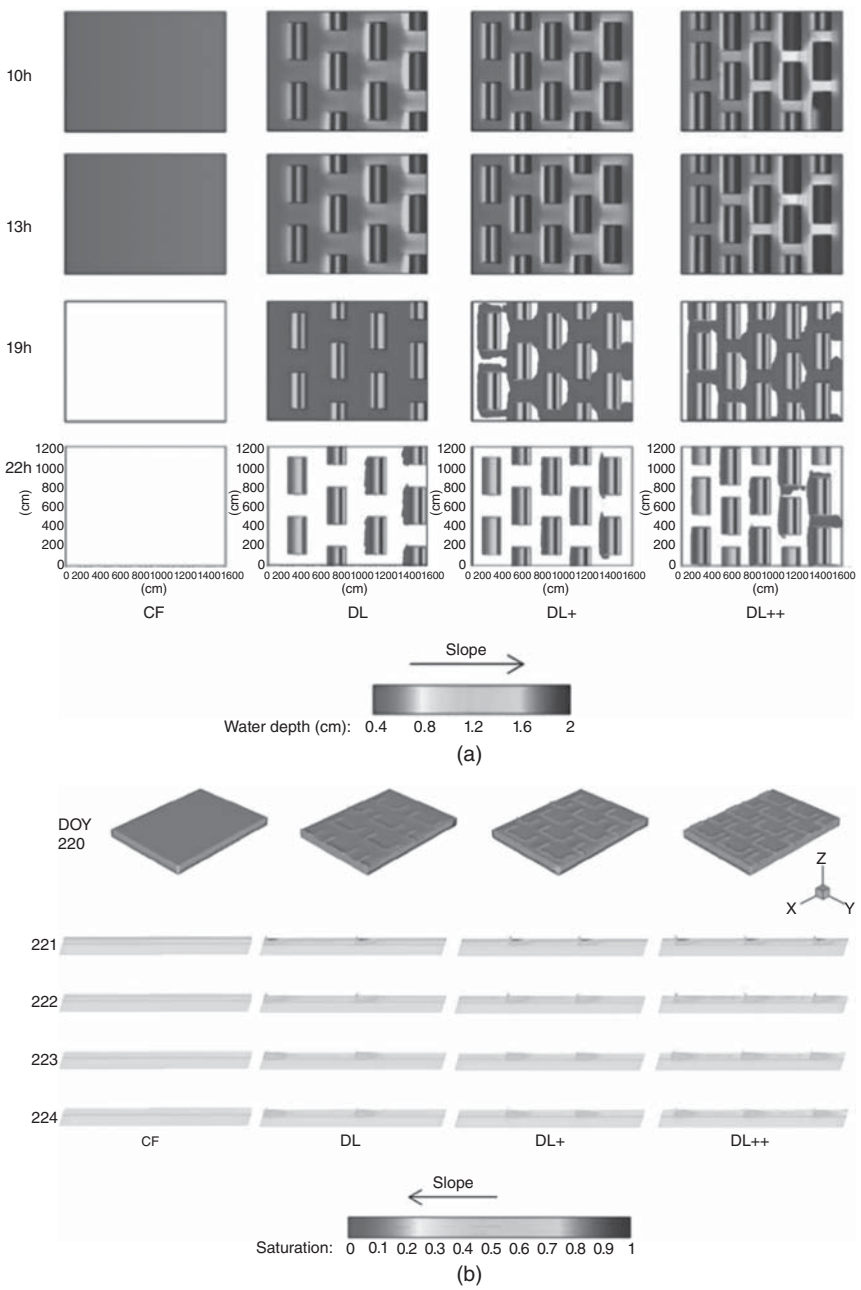

Figure 4.13 Simulated (a, left panel) water depth (overland flow) and (b, right panel) degree of saturation (subsurface flow) at different time steps following a rainfall event initiated at 07h on DOY 220 (40 mm) in 2011. CF is control, DL is original demi lunes (DL) design, DL+ and DL++ are optimized designs. White color in (a) means zero water depth and no overland flow; the lower part in (b) shows slices of the soil domain at y = 6 m for CF, DL and DL+ and at y = 7 m for DL++. DOY is day of the year from the Julian calendar. Source: Wildemeersch (2014).

half-moon *demi lunes* microcatchments (DL) in comparison with the control (CF). In DL, bunds were spaced at 4 m distance along the slope and 2 m across the slope or along the contour (Figure 4.12). The catchment (impluvium) to cropping area ratio was then 3 : 1, which is the upper limit of the range of 1 : 1 to 3 : 1 suggested by Chritchley and Siegert (1991) for microcatchments. Field trials had shown that the spacing of the microcatchments was not efficient in harvesting water and that the planting density within their cropping area was too high (24 plant pockets per cropping area). Increasing the number of microcatchments per field plot, while reducing planting density inside each cropping area, was therefore tested. Two modified microcatchment designs, DL+ and DL++, were introduced. DL+ and DL++ had 19 and 16 plant pockets per cropping area, respectively. The bund distance along the slope was reduced to 3 m in case of DL+ and in addition to that, the distance between bunds along the contour was reduced to 1 m in case of DL++, resulting in a catchment to cropping area ratio of 2.2 : 1 and 1.7 : 1, respectively. The plant density over the complete field plot thus remained at 10 000 plants ha^{-1} in all scenarios. The water balance components

of both designs was computed with the calibrated HGS (Wildemeersch 2014) (Figure 4.13).

In the left panel of Figure 4.13, two-dimensional illustrations of surface water depth (top views) are given for different time steps following a rain event on DOY 220 (40 mm) in 2011. Under CF, surface water runs off at the downslope side of the field, whereas for DL, DL+, and DL++, surface water is collected inside the DL cropping areas, resulting in increased water depths. Moreover, surface flow was redistributed from one DL cropping area to the other until surface flow stopped and water remained stagnant in the cropping area. Cross-sections along the slope clearly show higher soil–water contents in the soil profile for DL, DL+, and DL++ than for CF. The right panel of Figure 4.13 illustrates the evolution of soil–water contents in the subsurface as affected by treatment. Cross-sections along the slope clearly show higher soil moisture contents in the soil profile for DL, DL+, and DL++ than for C (Wildemeersch 2014).

Simulated surface evaporation did not vary much among treatments but was overall rather high (45–64% of total rainfall amount). Simulated runoff significantly reduced when microcatchment density per surface area increased. Runoff decreased from 37% to 50% of the total rainfall amount for the control to 28–42% for DL, 25–40% for DL+, and 23–37% for DL++. No rainfall water was lost as deep drainage (D = 0 at depth of 1.05 m). The actual transpiration remained overall low (<16% of rainfall) but increased with increasing DL microcatchment density. In the drier than normal 2011, soil–water depleted for all treatments over the 0–1.05 m, but in the wetter than normal year 2012 only CF resulted in soil–water depletion (Wildemeersch 2014).

4.6 Conclusions

In this chapter, four water harvesting studies in which a fully coupled surface–subsurface process-based hydrological model (HGS) was used have been presented. Two cases were from Latin America (Chile) and two from sub-Saharan Africa (Ethiopia and Niger). With the model being originally developed to simulate surface–subsurface water flow and solute transport at a larger watershed scale, this chapter describes the first attempts to apply it for evaluating and improving water harvesting techniques at the field and small watershed scale. Whereas water harvesting studies are often based on a trial and error approach or at best on an empirical approach, the approach presented here has many advantages and provides a better understanding of water flow processes at or near water harvesting techniques.

It was found that including at least two different data types to calibrate HGS, i.e. runoff hydrographs and soil–water content time series, resulted in the best agreement between observations and simulations (case 1 and 2 – Section 4.3 and case 3 – Section 4.4). However, including only soil–water content data also gave rise to reasonable results (case 4 – Section 4.5). Likewise, using detailed rain intensity values (Section 4.3) is better than using only average values (Sections 4.4 and 4.5), though the latter seemed acceptable. In case 1, 2, and 4, soil-moisture sensors (Section 4.3) or probes (Section 4.5) were used to measure soil–water content continuously or at regular time intervals, respectively, whereas in case 3 (Section 4.4), it was measured gravimetrically. Measuring soil–water content at regular time intervals (e.g. seven days) seemed appropriate. This shows that though complex mechanistic models are typically data demanding, using limited data was acceptable under the conditions tested in our cases. Yet, the model needs hydraulic properties (soil–water retention and hydraulic conductivity curves) which in our four cases where effectively measured in the field and in the lab. The model showed good results at both scales considered here, i.e. the field scale (cases 1, 3, and 4 – Sections 4.3, 4.4, and 4.5) and a 3-ha watershed scale (case 2 – Section 4.3).

The model appeared to be very useful to evaluate and improve water harvesting techniques. In case 1 (Section 4.3), it was shown that infiltration trenches laid out by governmental bodies were not effective, not in dry years but also not in wet years. In cases 3 and 4 (Sections 4.4 and 4.5, respectively), it was shown that improving the design of the water harvesting techniques resulted in significant lower runoff values when increasing furrow depth (case 3), but also allowed lower plant densities per microcatchment, while this did positively affect water harvesting (case 4). The model allows to compute all water balance components as well as relative yield.

The high performance of the model makes it very useful to conduct synthetic experiments and test a variety of combinations under historical and future weather conditions. Knowing how a given design performs under wet, normal, and dry years helps to effectively evaluate possible options. This is not possible with traditional field experiments. Produced outcomes can then be used as well to develop equations and determine parameter values that can be used in conceptual or engineering models.

As the model showed a reasonable performance at the watershed scale, it can be used to assess the upstream and downstream hydrological impact of water harvesting techniques. This is important as harvesting water upstream can deprive downstream water users, or can vice versa reduce flood risk and promote groundwater recharge and baseflow downstream.

References

Allen, R.G., Pereira, L.S., Raes, D., and Smith, M. (1998). *Crop Evapotranspiration: Guidelines for Computing Crop Requirements*. Irrigation and Drainage Paper No. 56. Rome, Italy: FAO.

Ammar, A.A. (2017) *Evaluating rainwater harvesting systems in arid and semi-arid regions*. PhD dissertation, Department Soil Physics and Land Management, Wageningen University and Research, the Netherlands.

Araya, T., Cornelis, W.M., Nyssen, J. et al. (2011). Effects of conservation agriculture on runoff, soil loss and crop yield under rain fed conditions in Tigray, Northern Ethiopia. *Soil Use and Management* 27: 404–414.

Araya, T., Nyssen, J., Govaerts, B. et al. (2015). Restoring cropland productivity and profitability in northern Ethiopian drylands after nine years of resource-conserving agriculture. *Experimental Agriculture* 52: 165–187.

Araya, T., Nyssen, J., Govaerts, B. et al. (2016). Seven years resource-conserving agriculture effect on soil quality and crop productivity in the Ethiopian drylands. *Soil and Tillage Research* 163: 99–109.

Baetens, J.M., Verbist, K., Cornelis, W.M. et al. (2009). On the influence of coarse fragments on soil water retention. *Water Resources Research* 45: W07408.

Boers, T.M. and Benasher, J. (1982). A review of rainwater harvesting. *Agricultural Water Management* 5: 145–158.

Boers, T.M., De Graaf, M., Feddes, R.A., and Ben-Asher, J. (1986). A linear regression model combined with a soil water balance model to design micro-catchments for water harvesting in arid zones. *Agricultural Water Management* 11: 187–206.

Chritchley, W. and Siegert, K. (1991). *Water Harvesting: A Manual for the Design and Construction of Water Harvesting Schemes for Plant Production*. Rome: FAO MISC/17/91.

Cornelis, W.M. (2014). Building resilience against drought: the soil-water management perspective. *Bulletins des Séances Académie Royale Sciences Outre-Mer/Mededelingen Zittingen Koninklijke Academie Overzeese Wetenschappen* 60: 465–482.

Cornelis, W.M., Corluy, J., Medina, H. et al. (2006). A simplified parametric model to describe the magnitude and geometry of soil shrinkage. *European Journal of Soil Science* 57: 258–268.

Cornelis, W.M., Verbist, K., McLaren, R.G., et al. (2012) 21st Century Hydrological Modeling for Optimizing Ancient Water Harvesting Techniques. AgroEnviron2012, 1–4 May 2012, Wageningen, the Netherlands. 5 p.

Cresswell, H.P., Bond, W.J., Simpson, R.J. et al. (2002). Soil water balance of three temperate pasture systems in Southern Australia. In: *Soil Physical Measurement and Interpretation for Land Evaluation* (eds. McKenzie, N., K. Coughlan, H. Cresswell, et al.), 332–343. Collingwood: CSIRO Publishing.

Dile, Y.T., Karlberg, L., Temesgen, M., and Rockström, J. (2013). The role of water harvesting to achieve sustainable agricultural intensification and resilience against water related shocks in sub-Saharan Africa. *Agriculture, Ecosystems and Environment* 181: 69–79.

Doherty, J. (2010). *PEST, Model-Independent Parameter Estimation User Manual*, 5e. Oxley, Australia: Watermark Numerical Computing.

Eslamian, S., Davari, A., and Reyhani, M.N. (2017). Iranian Qanāts: an ancient and sustainable water resources utilization. In: *Underground Aqueducts Handbook* (eds. A.N. Angelakis et al.), 123–150. CRC Group: Taylor and Francis.

Feddes, R.A. and Raats, P.A.C. (2004). Parameterizing the soil–water–plant root system. In: *Unsaturated-Zone Modeling: Progress, Challenges, Applications*, Wageningen UR Frontis Series, vol. 6 (eds. R.A. Feddes, G.H. de Rooij, J.C. van Dam, et al.), 95–141. Kluwer Academic Publishers.

Freeze, R.A. and Harlan, R.L. (1969). Blueprint for a physically-based digitally simulated, hydrological response model. *Journal of Hydrology* 9: 237–258.

Greve, P., Orlowsky, B., Mueller, B. et al. (2014). Global assessment of trends in wetting and drying over land. *Nature Geoscience* 7: 716–721.

Kristensen, K.J. and Jensen, S.E. (1975). A model for estimating actual evapotranspiration 825 from potential evapotranspiration. *Nordic Hydrology* 6: 170–188.

Lanckriet, S., Araya, T., Derudder, B. et al. (2014). Toward practical implementation of conservation agriculture: a case study in the May Zeg-zeg catchment (Ethiopia). *Agroecology and Sustainable Food Systems* 38: 913–935.

Makurira, H., Savenije, H.H.G., Uhlenbrook, S. et al. (2007). Towards a better understanding of water partitioning processes for improved smallholder rainfed agricultural systems: a case study of Makanya catchment, Tanzania. *Physics and Chemistry of the Earth* 32: 1082–1089.

McLaren, R.G. (2007) *Grid Builder. A pre-processor for 2-D, triangular element, finite element programs*. Groundwater Simulations Group, University of Waterloo, Canada.

Mualem, Y. (1976). A new model for predicting the hydraulic conductivity of unsaturated porous media. *Water Resources Research* 12: 513–522.

Okhravi, S.S., Eslamian, S.S., and Dalezios, N.R. (2019). Reducing water shortage crisis through rainwater reuse: lessons learned from ancient toward integrated technology. *International Journal of Hydrology Science and Technology* 9: 587–602.

Opolot, E. (2012) *Evaluating in-situ soil water conservation practices with a fully-coupled surface/subsurface process-based hydrological model in Tigray, Ethiopia*. MSc dissertation, Department of Soil Management, Ghent University, Belgium.

Opolot, E., Araya, T., Nyssen, J. et al. (2016). Evaluating in situ water and soil conservation practices with a fully-coupled, surface/subsurface process-based hydrological model in Tigray, Ethiopia. *Land Degradation and Development* 27: 1781–1872.

Ouessar, M., Bruggeman, A., Abdelli, F. et al. (2009). Modelling water-harvesting systems in the arid south of Tunisia using SWAT. *Hydrology and Earth System Sciences* 13: 2003–2021.

Pandey, D.N., Gupta, A.K., and Anderson, D.M. (2003). Rainwater harvesting as an adaptation to climate change. *Current Science* 85: 46–59.

Rockström, J. and Falkenmark, M. (2015). Agriculture: increase water harvesting in Africa. *Nature* 519: 283–285.

Sillmann, J., Kharin, V.V., Zwiers, F.W. et al. (2013). Climate extremes indices in the CMIP5 multimodel ensemble: part 2. Future climate projections. *Journal of Geophysical Research: Atmospheres* 118: 2473–2493.

Sivakumar, M. (1989). Agroclimatic aspects of rainfed agriculture in the Sudano-Sahelian zone. In: *Soil, Crop and Water Managements Systems for Rainfed Agriculture in the Sudano-Sahelian Zone*. Proceedings of an International Workshop, ICRISAT Sahelian Center, Niamey, Niger, 7–11 January 1987, ICRISAT, Patancheru, A.P. 502324, India, 17–38.

Steduto, P., Hsiao, T.C., Raes, D., and Fereres, E. (2009). AquaCrop – the FAO crop model to simulate yield response to water: I. Concepts and underlying principles. *Agronomy Journal* 101: 426–437.

Stroosnijder, L. (2009). Modifying land management in order to improve efficiency of rainwater use in the African highlands. *Soil and Tillage Research* 103: 247–256.

Sudicky, E., Jones, J., Park, Y.-J. et al. (2008). Simulating complex flow and transport dynamics in an integrated surface-subsurface modeling framework. *Geosciences Journal* 12: 107–122.

Therrien, R., McLaren, R.G., Sudicky, E.A., and Panday, S.M. (2010). *HydroGeoSphere, A Three-Dimensional Numerical Model Describing Fully-Integrated Subsurface and Surface Flow and Solute Transport : User's Guide*. Waterloo ON, Canada: Groundwater Simulations Group 467 p.

Van Genuchten, M.T. (1980). A closed-form equation for predicting the hydraulic conductivity of unsaturated soils. *Soil Science Society of America Journal* 44: 892–898.

Verbist, K., Schiettecatte, W., and Gabriels, D. (2003). Usability of rainfall simulation experiments to assess soil erosion under natural rainfall. In: *25 Years of Assessment of Erosion* (eds. D. Gabriels and W.M. Cornelis), 269–276. Ghent, Belgium: Ghent University.

Verbist, K., Baetens, J.M., Cornelis, W.M. et al. (2009). Hydraulic conductivity as influenced by stoniness in degraded drylands of Chile. *Soil Science Society of America Journal* 73: 471–484.

Verbist, K., Robertson, A., Cornelis, W.M., and Gabriels, D. (2010a). Seasonal predictability of daily rainfall characteristics in Central-Northern Chile for dry-land management. *Journal of Applied Meteorology and Climatology* 49: 1938–1955.

Verbist, K., Torfs, S., Cornelis, W.M. et al. (2010b). Comparison of single- and double-ring infiltrometer methods on stony soils. *Vadose Zone Journal* 8: 462–475.

Verbist, K., Pierreux, S., Cornelis, W.M. et al. (2012). Parameterizing a coupled surface-subsurface three-dimensional soil hydrological model to evaluate the efficiency of a runoff water harvesting technique. *Vadose Zone Journal* https://doi.org/10.2136/vzj2011.0141.

Wani, S.P., Sreedevi, T.K., Rockström, J., and Ramakrishna, Y.S. (2009). Rainfed agriculture – past trends and future prospects. In: *Rainfed Agriculture: Unlocking the Potential* (eds. S.P. Wani et al.), 1–35. CAB International.

Wigmosta, M.S., Vail, L.W., and Lettenmaier, D.P. (1994). A distributed hydrology vegetation model for complex terrain. *Water Resources Research* 30: 1665–1679.

Wildemeersch, J. (2014) *Integrated biophysical and socio-economic evaluation of water and soil conservation techniques: a case study from Niger*. PhD dissertation, Department of Soil Management, Ghent University, Belgium.

Wildemeersch, J., Garba, M., Sabiou, M. et al. (2015a). Agricultural drought trends and mitigation in Tillaberí, Niger. *Soil Science and Plant Nutrition* 61: 414–425.

Wildemeersch, J., Garba, M., Sabiou, M. et al. (2015b). The effect of water and soil conservation (WSC) on the soil chemical, biological and physical soil quality of a Plinthosol in Niger. *Land Degradation and Development* 26: 773–783.

Wöhling, T. and Vrugt, J.A. (2011). Multiresponse multilayer vadose zone model calibration using Markov chain Monte Carlo simulation and field water retention data. *Water Resources Research* 47: W04510.

Wu, P., Christidis, N., and Stott, P. (2013). Anthropogenic impact on Earth's hydrological cycle. *Nature Climate Change* 3: 807–810.